Linear instability in a miscible core-annular flow of a Newtonian and a Bingham fluid

Kirti Chandra Sahu*
Department of Chemical Engineering, Indian Institute of Technology Hyderabad, Kandi, Sangareddy 502 285, Telangana, India
(Dated: October 29, 2018)

The linear instability characteristics of a core-annular pipe flow of a Newtonian fluid and a Bingham fluid separated by a mixed region is investigated. The main objective of this study is to investigate the effect of the yield stress of the annular fluid on the stability behaviour. The present linear stability analysis reveals that the corkscrew mode is the most dangerous mode for the parameters considered. The Bingham number seems to destabilise the flow via modifying the velocity profile. The mechanism of instability is found to be inviscid in nature. An energy budget analysis shows that the energy due to the gradient of viscosity perturbation in the radial direction, and the transfer of energy from the basic flow to the perturbation via the "Reynolds stress" term are responsible for the instability observed. The positive contributions of these terms towards instability increases with increasing the yield stress. The critical Reynolds number also decreases with increasing the Bingham number for the corkscrew mode, which indicates the destabilising influence of the yield stress.

I. INTRODUCTION

The study of linear instability of miscible and immiscible fluids has received considerable attention in literature experimentally, theoretically, and numerically due to their relevance in many industrial applications and natural phenomena. An extensive review of instabilities in viscosity-stratified systems can be found in Govindarajan & Sahu [1]. In the oil and gas industry, the transportation of crude oil in pipelines relies on the stability of core-annular pipe flows [2]. In the chemical process industry, the stability of miscible flows features in center line injectors [3]. In the food and drink industry, cleaning of plants involves the removal of a highly viscous fluid by fast-flowing water streams. In many of these situations, the working fluids do not obey Newton's law of viscosity, and hence termed as non-Newtonian fluids. Several non-Newtonian models have been proposed to deal with the rheology of such fluids. A common feature of these fluids is the appearance of a yield stress. This concept has been challenged in the past by many researchers, but remains a very useful approximation [4, 5].

First, instabilities in core-annular/three-layer flows of Newtonian fluids in pipes or channels are discussed. In the following, the emphasis has been given to the linear stability studies associated with miscible fluids; however, a large number of investigations in the past have also focused on the stability of immiscible fluids in both planar and cylindrical geometries (see for instance [6–10]). Govindarajan and co-workers [11, 12] studied a three-layer channel flow by conducting a linear stability analysis. They showed that the flow is stabilised when the near wall fluid is less viscous than the fluid in the central region of the channel, and vice versa. The stability behaviour is studied with respect to a single fluid flow in a channel, in which the flow is linearly unstable when the Reynolds number based on centerline velocity and channel height is greater than 5772.2. Sahu *et al.* [13] found that the flow is absolutely unstable (i.e. the disturbance grows in both downstream and upstream directions) for high viscosity ratios. These studies were extended to double-diffusive systems (where viscosity-stratification is accomplished due to the presence of two species with different diffusivities) by Sahu & Govindarajan [14] in a channel. They found the existence of an additional unstable mode due to the differential diffusivity of the species at low Reynolds number, in addition to the standard Tollmien-Schlichting (TS) unstable mode. In the case of a cylindrical configuration (core-annular flow) involving Newtonian fluids, several authors [15–18] have examined the development of axisymmetric and corkscrew patterns, which were also verified experimentally by d'Olce *et al.* [19]. Selvam *et al.* [20] conducted linear stability analysis of a core-annular flow in a pipe, and showed that the axisymmetric (corkscrew) mode is dominant if the annular fluid is less (more) viscous than the core fluid. However, in case of single fluid flow in a pipe (the Hagen-Poiseuille flow), the corkscrew mode is always the least stable one. This case is known to be linearly stable at any Reynolds number.

Next, the previous studies involving the linear stability of non-Newtonian fluids are discussed. The linear stability of a two-layer channel flow of two Bingham fluids was studied by Frigaard *et al.* [21]. Considering two-dimensional disturbance in their normal mode analysis, they showed that increasing yield stress stabilises the flow. In the configuration studied by Frigaard *et al.* [21], the unyielded region between the fluids suppresses the interfacial mode leading to a super-stable two-layer flow. A similar conclusion was also achieved in case of a plane Poiseuille flow of a Bingham

* ksahu@iith.ac.in

fluid [22], and a two-layer Poiseulle flow of Carreau-Yasuda and Bingham fluids [23]. Frigaard and Nouar [24] and Sahu *et al.* [25] realised that Squire's theorem (which states that two-dimensional disturbance is more unstable than the corresponding three-dimensional disturbance at the same Reynolds number) is not valid for non-Newtonian fluids and conducted linear stability analyses of a plane Poiseuille flow of a Bingham fluid and a two-layer channel flow of Newtonian and Herschel-Bulkley fluids, respectively. They found the existence of three-dimensional instability in these situations. Unlike Frigaard *et al.*, [22], Sahu *et al.* [26] showed that when the non-Newtonian layer is yielded completely, the Bingham number has a destabilising influence in a two-layer channel flow.

The above-mentioned investigations focused on plane channel flows of non-Newtonian immiscible fluids (surface-tension acts at the interface separating the fluids). However, there are few studies which experimentally investigated the flow instability in cylindrical pipes as well [27–31] by considering yield stress and shear thinning fluids. Figaard and co-authors [32–34] also study the instability in core-annular flows of two immiscible fluids by an energy stability analysis and experimentation. They investigated interfacial instability for different radii of the core fluid and the thicknesses of the plug region. The objective of the present study is to investigate the linear instability in a core-annular flow of a Newtonian fluid and a Bingham fluid in a cylindrical pipe. The fluids are considered to be miscible, which is characterised by diffusivity/Schmidt number. To the best of my knowledge, the present work is a first attempt to investigate linear instability of a Newtonian and a Bingham fluid separated by a mixed region in a core-annular pipe flow configuration. An energy budget analysis and inviscid stability theory are also conducted to understand the underlying mechanism of this instability.

The rest of this paper is organised as follows. The problem is formulated and the governing linear stability equations are derived in Section II. The results obtained from the linear stability analysis are discussed in Section III, wherein a parametric study is conducted to investigate the effects of the Bingham number, the Schmidt number and the viscosity ratio. Concluding remarks are provided in Section IV.

II. FORMULATION

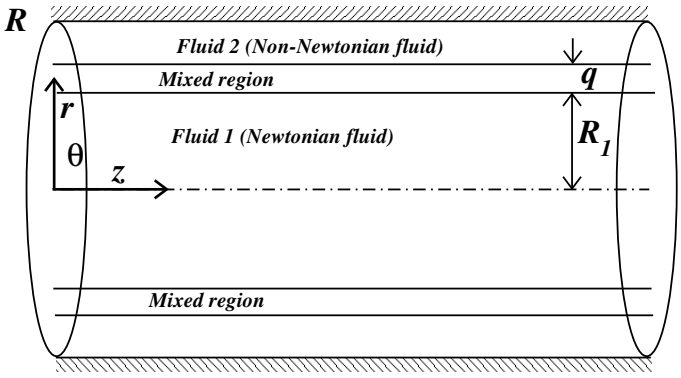

FIG. 1: Schematic of the flow configuration considered. The core fluid ($0 \leq r \leq R_1$), designated by fluid '1', is a Newtonian fluid, and the annular fluid ($R_1 + q < r < R$), designated by fluid '2', is a non-Newtonian fluid. The fluids are separated by a mixed layer of uniform thickness q.

The linear stability characteristics of a pressure-driven core-annular flow of two miscible fluids in a rigid and impermeable pipe of radius R is considered. A schematic diagram of the flow system is shown in Fig. 1. The core fluid (fluid '1', in region $0 \leq r \leq R_1$) is a Newtonian fluid, whereas the annular fluid (fluid '2', in region $R_1 + q \leq r \leq R$) is a non-Newtonian fluid. The fluids are separated by a mixed layer of uniform thickness q. A parallel flow approximation is employed in prescribing the thickness q to be uniform [35]. A cylindrical coordinate system (r, θ, z), where r, θ and z denote the radial, the azimuthal and the axial coordinates, respectively, is used.

In order to isolate the effect of viscosity stratification, the density (ρ) of the fluids are assumed to be the same. The viscosity of fluid '1' and fluid '2' are μ_1 and μ_2, respectively. The viscosity of the non-Newtonian fluid (μ_2) is characterised by a Bingham fluid model [36, 37]:

$$\mu_2 = k + \tau_0 |\Pi|^{-1}, \tag{1}$$

where k denotes the plastic viscosity and τ_0 is the yield shear stress. The second invariant of the rate of strain tensor,

$\Pi = (2E_{ij}E_{ij})^{1/2}$, can be written in the expanded form as

$$\Pi^2 = 2\left[\left(\frac{\partial u_r}{\partial r}\right)^2 + \left(\frac{1}{r}\frac{\partial u_\theta}{\partial \theta} + \frac{u_r}{r}\right)^2 + \left(\frac{\partial u_z}{\partial z}\right)^2\right] + \left[r\frac{\partial}{\partial r}\left(\frac{u_\theta}{r}\right) + \frac{1}{r}\frac{\partial u_r}{\partial \theta}\right]^2 + \left(\frac{\partial u_r}{\partial z} + \frac{\partial u_z}{\partial r}\right)^2 + \left(\frac{1}{r}\frac{\partial u_z}{\partial \theta} + \frac{\partial u_\theta}{\partial z}\right)^2, \quad (2)$$

where $E_{ij} = \frac{1}{2}(\partial u_i/\partial x_j + \partial u_j/\partial x_i)$; $\mathbf{u} \equiv (u_r, u_\theta, u_z)$ is the velocity vector, and u_r, u_θ and u_z are the velocity components in the the radial (r), the azimuthal (θ) and the axial (z) directions, respectively.

A. Governing equations

The flow dynamics is governed by the incompressible form of the continuity and the Navier-Stokes equations, in addition to a convection-diffusion equation of the volume-fraction of the Bingham fluid, s.

$$\nabla \cdot \mathbf{u} = 0, \quad (3)$$

$$\rho\left[\frac{\partial \mathbf{u}}{\partial t} + \mathbf{u}\cdot\nabla\mathbf{u}\right] = -\nabla p + \nabla\cdot\left[\mu(\nabla\mathbf{u} + \nabla\mathbf{u}^T)\right], \quad (4)$$

$$\frac{\partial s}{\partial t} + \mathbf{u}\cdot\nabla s = \mathcal{D}_s\nabla^2 s, \quad (5)$$

where t denotes time, p represents pressure field, and $\mathcal{D}_s$ is the diffusion coefficient of the scalar, s.

The governing equations are nondimensionalised using the radius of the pipe (R) as the length scale and the average velocity, $V \equiv Q/\pi R^2$ as the velocity scale. The following scaling is employed to render the governing equations dimensionless:

$$(r, z, q, R_1) = R\left(\widetilde{r}, \widetilde{z}, \widetilde{q}, \widetilde{R}_1\right),\ t = \frac{R}{V}\widetilde{t},\ (u_r, u_\theta, u_z) = V\left(\widetilde{u}_r, \widetilde{u}_\theta, \widetilde{u}_z\right),\ p = \rho V^2\widetilde{p},\ \mu = \widetilde{\mu}\mu_1, \quad (6)$$

where tildes designate dimensionless quantities. After dropping the tildes decoration, the dimensionless governing equations are given by

$$\nabla \cdot \mathbf{u} = 0, \quad (7)$$

$$\frac{\partial \mathbf{u}}{\partial t} + \mathbf{u}\cdot\nabla\mathbf{u} = -\nabla p + \frac{1}{Re}\nabla\cdot\left[\mu(\nabla\mathbf{u} + \nabla\mathbf{u}^T)\right], \quad (8)$$

$$\frac{\partial s}{\partial t} + \mathbf{u}\cdot\nabla s = \frac{1}{ReSc}\nabla^2 s, \quad (9)$$

where $Re(\equiv \rho VR/\mu_1)$ and $Sc(\equiv \mu_1/\rho\mathcal{D}_s)$ are the Reynolds number and the Schmidt number, respectively. The dimensionless viscosity, μ is given by

$$\mu = (1-s) + s\left[m + Bn|\Pi_0|^{-1}\right], \quad (10)$$

where $Bn\,(\equiv \tau_0 R/\mu_1 V)$ and $m(\equiv k/\mu_1)$ are the Bingham number and the Newtonian viscosity ratio, respectively. In literature, both linear and exponential viscosity-concentration relationships were used (see e.g. [38]). Here, it is found that changing the viscosity-concentration relationship do not change the instability results qualitatively. Therefore, the simplest form of viscosity-concentration dependence has been chosen in the present study.

B. Basic state

The basic state whose linear stability characteristics will be analyzed, corresponds to a steady, parallel, fully-developed flow, i.e. $U_r = U_\theta = 0; U_z = U_z(r)$, and P is linear in z. The basic state is obtained by solving the steady, fully-developed version of Eq. (8), i.e.,

$$\frac{1}{r}\frac{d}{dr}\left[r\mu_0\frac{dU_z}{dr}\right] = \frac{dP}{dz}Re, \quad (11)$$

subject to the no-slip and symmetric boundary conditions at the wall ($r = 1$) and the centerline ($r = 0$) of the pipe, respectively. Note that the basic state profile, given by Eq. (11), is a function of $(dP/dz)Re$, which is obtained

from the constant volumetric flow condition, such that dimensionless average velocity, $V = Q/2\pi \int_0^1 r dr = 1$, which implies that $2\int_0^1 U_z r dr = 1$. Thus, when the constant volumetric flow condition is applied, the velocity profiles become independent of Re. In other words, for a given value of Re, the pressure-gradient gets adjusted such that $V = 1$. The basic state quantities are designated by upper-case letters for the flow variables, and by the subscript 0 for viscosity and s. The second invariant of the rate of strain tensor for the basic state, $\Pi_0 = dU_z/dr$. Without loss of generality, the value of s_0 can be assumed to be 0 and 1 for the Newtonian (fluid '1') and the Bingham (fluid '2') fluids, respectively. The following variation of s_0 can be assumed, such that s_0 is continuous upto the second derivative everywhere across the domain.

$$\begin{aligned} s_0 &= 0, \qquad 0 \le r \le R_1, \\ s_0 &= \sum_{i=1}^{6} a_i r^{i-1}, \quad R_1 \le r \le R_1 + q, \\ s_0 &= 1, \qquad R_1 + q \le r \le 1, \end{aligned} \tag{12}$$

where a_i $(i = 1, 6)$ are given by

$$\begin{aligned} a_1 = -\frac{{R_1}^3}{q^5}\left(6R_1^2 + 15R_1 q + 10q^2\right), \quad a_2 = \frac{30{R_1}^2}{q^5}(R_1+q)^2, \\ a_3 = -\frac{30R_1}{q^5}(R_1+q)(2R_1+q), \quad a_4 = \frac{10}{q^5}\left(6R_1^2 + 6R_1 q + q^2\right), \\ a_5 = -\frac{15}{q^5}(2R_1+q) \quad \text{and} \quad a_6 = \frac{6}{q^5}. \end{aligned} \tag{13}$$

It has been confirmed that the use of other sufficiently smooth profiles does not change the stability characteristics of the system considered. It is to be noted here that such a profile does not satisfy Eq. (5) as when two fluids of different concentration come into contact and slowly diffuse into each other, under the boundary layer approximation they will attain an error function profile. However, it was shown by several researchers in the past [38, 39] that the stability characteristics obtained using the above-mentioned type profile and an error function profile for s_0 are indistinguishable. We observe a similar behaviour in the present study as well. Also the locally parallel assumption, i.e the variation of s_0 in the r direction is much larger than its growth the z direction, used to obtain the basic state in the present study implies that the variation of the gradients of the flow variables and the thickness q of the mixed region have much larger length scale than the most-unstable disturbance wavelength. Such flows are not uncommon in chemical industry, and for example Joseph & Renardy [51, 52] show many such real-life situations of nearly parallel flow of two miscible fluids with a thin and very slowly growing mixed layer between them. In such a scenario, the concentration is a function of r and t only and not of z. The justification of the parallel flow approximation and the basic state concentration profile (Eq. 12) used in the present study are also discussed in Appendix.

The basic state viscosity, μ_0 is given by

$$\mu_0 = (1 - s_0) + s_0\left[m + Bn|\Pi_0|^{-1}\right]. \tag{14}$$

As the volumetric flow rate is kept constant, the basic state depends on the location of the mixed layer (R_1), mixed layer thickness (q), the Newtonian viscosity ratio (m) and the Bingham number (Bn). Typical basic state profiles of axial velocity (U_z), U_z' and viscosity (μ_0) are shown for different values of Bn in Fig. 2(a), (b) and (c), respectively. The rest of the parameters are chosen as $R_1 = 0.55$, $q = 0.1$ and $m = 10$. It is to be noted here that for a given set of dimensionless parameters, as the value of Bn exceeds a critical value (Bn_{cr}), the velocity profile becomes unphysical due to the appearance of unyielded region in the Bingham layer [22, 34]. This is also explained in detail in the Appendix and presented in Fig. 13. The value of $Bn_{cr} \approx 15$ for $m = 10$; it is found that decreasing m decreases Bn_{cr} for fixed values of R_1 and q. It will be seen in Fig. 5(a) that for $m = 1$, $Bn_{cr} = 7$. In Fig. 2(a) and (b), it can be seen that increasing the value of Bn decreases in the gradient of velocity U_z at $r = R_1$. In the mixed region ($R_1 < r < R_1 + q$), U_z' increases as expected, and again decreases in the Bingham layer ($R_1 + q \le r \le 1$) due to the increase in the shear. This behaviour is supplemented by a sharp increase in viscosity (μ_0) at $r = R_1$, which decreases gradually in the Bingham layer (see Fig. 2(c)). These features indicate that the Bingham number will have a strong influence on the instability behaviour of the core-annular flow of two miscible fluids.

C. Linear stability equations

A temporal stability analysis is conducted of the basic flow given by Eqs. (11)-(12) to infinitesimal perturbation. A normal mode form is used to express each flow variable as a sum of the basic state and a time-dependent perturbation

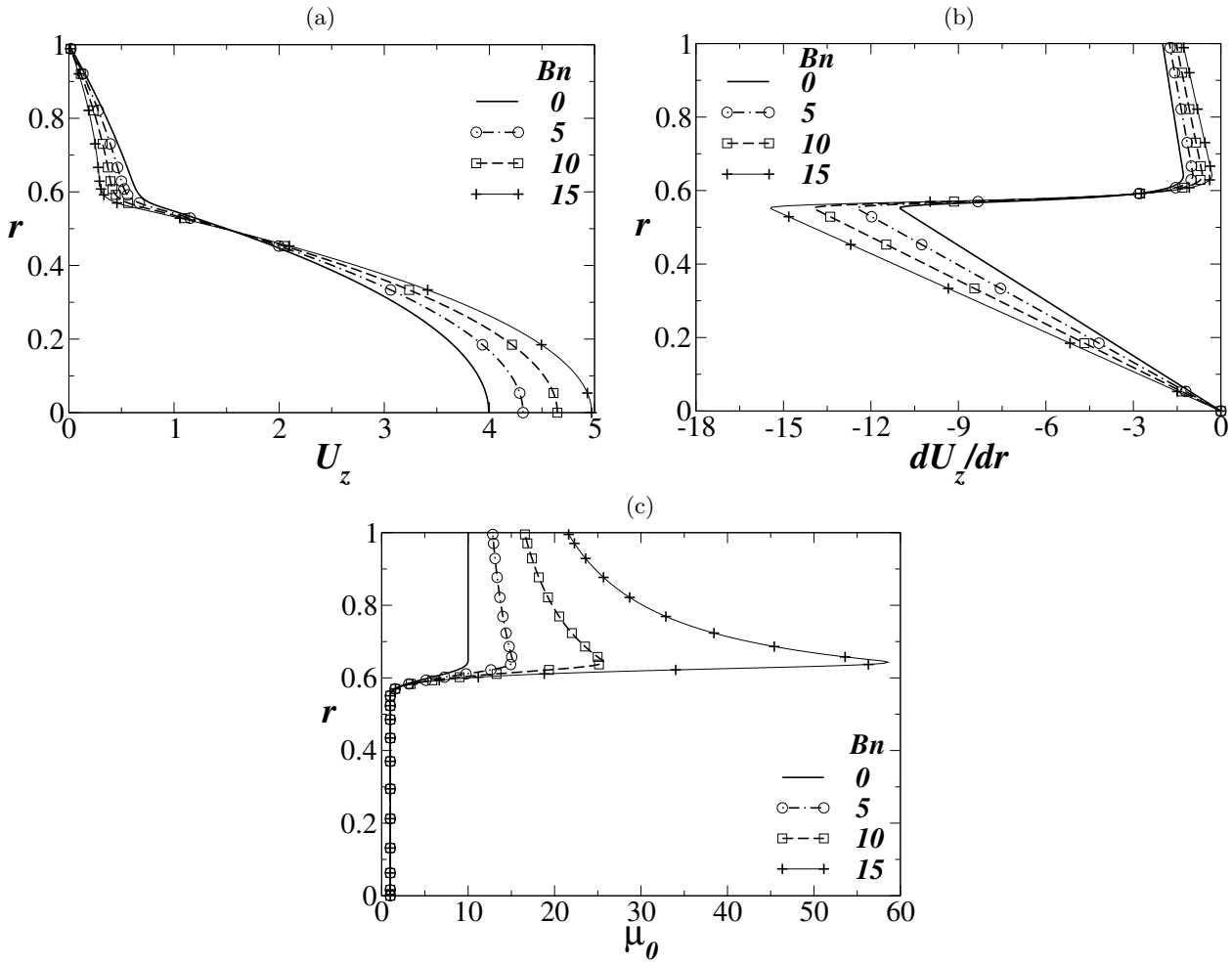

FIG. 2: Basic state profiles of (a) axial velocity (U_z), (b) gradient of U_z in the radial direction, (U_z'), and (c) viscosity (μ_0) for different values of Bn. The rest of the parameter values are $R_1 = 0.55$, $q = 0.1$ and $m = 10$.

(designated by a hat):

$$(u_r, u_\theta, u_z, p, s, \pi)(r, \theta, z, t) = (0, 0, U_z(r), P, s_0(r), \Pi_0) + (\mathrm{i}\hat{u}_r, \hat{u}_\theta, \hat{u}_z, \hat{p}, \hat{s}, \hat{\pi})(r) e^{\mathrm{i}(\alpha z + \beta\theta - \omega t)}, \tag{15}$$

where $\mathrm{i} \equiv \sqrt{-1}$, α, β and $\omega(\equiv \alpha c)$ are the wavenumbers (real) in the axial and the azimuthal directions, and the frequency (complex) of the perturbation, respectively, wherein $c(\equiv c_r + \mathrm{i}c_i)$ is the phase speed of the perturbation. The subscripts r and i represent the real and imaginary parts, respectively. By differencing the disturbance (last term in Eq. (15)) with respect to time, it can be shown that a given mode is unstable if $\omega_i > 0$, stable if $\omega_i < 0$ and neutrally stable if $\omega_i = 0$. By performing a Taylor-series expansion of the viscosity $\mu(s, \pi)$ about the basic state, the perturbation viscosity can be written as:

$$\hat{\mu} = \frac{\partial \mu_0}{\partial s_0}\hat{s} + \frac{\partial \mu_0}{\partial \Pi_0}\hat{\pi} \equiv R_s \hat{s} + R_\pi \hat{\pi}, \tag{16}$$

where $\hat{\pi} = -\alpha\hat{u}_r + \hat{u}_z'$. Following the standard procedure (see for instance Schmid & Henningson [40]): (i) substitution of Eq. (15) into Eqs. (7)-(9), (ii) subtraction of the basic state equations, and (iii) linearization and elimination of the pressure perturbation, result in the following linear stability equations (written after suppressing the hat notations), we obtain

$$-\omega u_r + \alpha u_r U_z = p' - \frac{\mathrm{i}}{Re}\Big[\mu_0 \left\{ u_r{}'' + \frac{u_r{}'}{r} - \left(\frac{\beta^2+1}{r^2} + \alpha^2\right) u_r - \frac{2\beta}{r^2} u_\theta \right\} + 2\mu_0' u_r{}' + \alpha U_z' \mu \Big], \tag{17}$$

$$-\omega u_\theta + \alpha u_\theta U_z = -\frac{\beta p}{r} - \frac{\mathrm{i}\mu_0}{Re}\left\{ u_\theta{}'' + \frac{u_\theta{}'}{r} - \left(\frac{\beta^2+1}{r^2} + \alpha^2\right) u_\theta - \frac{2\beta}{r^2} u_r \right\} - \frac{\mathrm{i}\mu_0{}'}{Re}\left[u_\theta{}' - \frac{u_\theta}{r} - \frac{\beta u_r}{r} \right], \tag{18}$$

$$-\omega u_z + U_z{}' u_r + \alpha U_z u_z = -\alpha p - \frac{\mathrm{i}\mu_0}{Re}\left\{u_z{}'' + \frac{u_z{}'}{r} - \left(\frac{\beta^2}{r^2}+\alpha^2\right)u_z\right\} - \frac{\mathrm{i}\mu_0'}{Re}\left[v_z' - \alpha v_r\right] - \frac{\mathrm{i}U_z'}{Re}\mu' - \frac{\mathrm{i}\mu}{Re}\left[U_z{}'' + \frac{U_z'}{r}\right], \tag{19}$$

$$u_r' + \frac{u_r}{r} + \frac{\beta u_\theta}{r} + \alpha u_z = 0, \tag{20}$$

$$-\omega s + s_0{}' u_r + \alpha U_z s = -\frac{\mathrm{i}}{ReSc}\left\{s'' + \frac{s'}{r} - \left(\frac{\beta^2}{r^2}+\alpha^2\right)s\right\}, \tag{21}$$

where the prime denotes differentiation with respect to r. Here it has been assumed that the growth of the mixed layer is associated with a much larger length scale than the disturbance wavelength. Thus, the diffusion and the advective terms would effect the disturbance, but not the basic concentration profile in accordance with the locally parallel assumption. It is confirmed that without viscosity-stratification, i.e. by setting $Bn = 0$ and $\mu_0 = 1$, these equations reduce to the stability equations for the Hagen-Poiseuille flow [40]. Solutions of these equations are obtained subject to the following boundary conditions [41]:

At the centerline of the pipe ($r = 0$), the boundary conditions are

$$u_r = 0,\ \ u_\theta = 0,\ \ u_z{}' = 0,\ \ p' = 0,\ \ s' = 0 \ \text{ and for } \ \beta = 0, \tag{22}$$

$$u_r + u_\theta = 0,\ \ 2u_r' + u_\theta' = 0,\ \ u_z = 0,\ \ p = 0,\ \ s = 0 \ \text{ and for } \ \beta = 1, \tag{23}$$

$$u_r = 0,\ \ u_\theta = 0,\ \ u_z = 0,\ \ p = 0,\ \ s = 0 \ \text{ and for } \ \beta \geq 2. \tag{24}$$

At the pipe wall ($r = 1$), the boundary conditions are

$$u_r = 0,\ \ u_\theta = 0,\ \ u_z = 0,\ \ s' = 0, \tag{25}$$

for all values of β. Eqs. (17)-(21) along with the boundary conditions (23)-(25) constitute an eigenvalue problem, given by

$$\begin{bmatrix} \mathcal{A}_{11} & \mathcal{A}_{12} & \mathcal{A}_{13} & \mathcal{A}_{14} & \mathcal{A}_{15} \\ \mathcal{A}_{21} & \mathcal{A}_{22} & 0 & \mathcal{A}_{24} & 0 \\ \mathcal{A}_{31} & 0 & \mathcal{A}_{33} & \mathcal{A}_{34} & \mathcal{A}_{35} \\ \mathcal{A}_{41} & \mathcal{A}_{42} & \mathcal{A}_{43} & 0 & 0 \\ \mathcal{A}_{51} & 0 & 0 & 0 & \mathcal{A}_{55} \end{bmatrix} \begin{bmatrix} u_r \\ u_\theta \\ u_z \\ p \\ s \end{bmatrix} = \omega \begin{bmatrix} 1 & 0 & 0 & 0 & 0 \\ 0 & 1 & 0 & 0 & 0 \\ 0 & 0 & 1 & 0 & 0 \\ 0 & 0 & 0 & 0 & 0 \\ 0 & 0 & 0 & 0 & 1 \end{bmatrix} \begin{bmatrix} u_r \\ u_\theta \\ u_z \\ p \\ s \end{bmatrix}, \tag{26}$$

where,

$$\begin{aligned}
\mathcal{A}_{11} &= \alpha U_z + \frac{\mathrm{i}\mu_0}{Re}\left\{\mathcal{D}^2 + \frac{\mathcal{D}}{r} - \left(\frac{\beta^2+1}{r^2}+\alpha^2\right)\right\} + \frac{2\mathrm{i}\mu_0'}{Re}\mathcal{D} - \frac{\mathrm{i}}{Re}\alpha^2 U_z{}' R_s,\ \ \mathcal{A}_{12} = -\frac{2\mathrm{i}\beta\mu_0}{r^2 Re}, \\
\mathcal{A}_{13} &= \frac{\mathrm{i}}{Re}\alpha U_z{}' R_\pi \mathcal{D},\ \ \mathcal{A}_{14} = -\mathcal{D},\ \ \mathcal{A}_{15} = \frac{\mathrm{i}U_z'\alpha}{Re}R_s, \\
\mathcal{A}_{21} &= -\frac{2\mathrm{i}\beta\mu_0}{r^2 Re} - \frac{\mathrm{i}\beta\mu_0'}{rRe},\ \ \mathcal{A}_{22} = \alpha U_z + \frac{\mathrm{i}\mu_0}{Re}\left\{\mathcal{D}^2 + \frac{\mathcal{D}}{r} - \left(\frac{\beta^2+1}{r^2}+\alpha^2\right)\right\} + \frac{\mathrm{i}\mu_0'}{Re}\left(\mathcal{D} - \frac{1}{r}\right),\ \ \mathcal{A}_{24} = \frac{\beta}{r}, \\
\mathcal{A}_{31} &= U_z' - \frac{\mathrm{i}\mu_0'\alpha}{Re} - \frac{\mathrm{i}U_z'\alpha}{Re}\left(R_\pi' + R_\pi\mathcal{D}\right) - \frac{\mathrm{i}\alpha}{Re}\left(U_z'' + \frac{U_z'}{r}\right)R_\pi, \\
\mathcal{A}_{33} &= \alpha U_z + \frac{\mathrm{i}\mu_0}{Re}\left\{\mathcal{D}^2 + \frac{\mathcal{D}}{r} - \left(\frac{\beta^2}{r^2}+\alpha^2\right)\right\} + \frac{\mathrm{i}\mu_0'}{Re}\mathcal{D} + \frac{\mathrm{i}U_z'}{Re}\left(R_\pi'\mathcal{D} + R_\pi\mathcal{D}^2\right) + \frac{\mathrm{i}}{Re}\left(U_z'' + \frac{U_z'}{r}\right)R_\pi\mathcal{D}, \\
\mathcal{A}_{34} &= \alpha,\ \ \mathcal{A}_{35} = \frac{\mathrm{i}U_z'}{Re}\left(R_s' + R_s\mathcal{D}\right) + \frac{\mathrm{i}R_s}{Re}\left(U_z'' + \frac{U_z'}{r}\right),\ \ \mathcal{A}_{41} = \mathcal{D} + \frac{1}{r},\ \ \mathcal{A}_{42} = \frac{\beta}{r},\ \ \mathcal{A}_{43} = \alpha, \\
\mathcal{A}_{51} &= s_0',\ \ \mathcal{A}_{55} = \alpha U_z + \frac{\mathrm{i}}{ReSc}\left\{\mathcal{D}^2 + \frac{\mathcal{D}}{r} - \left(\frac{\beta^2}{r^2}+\alpha^2\right)\right\}.
\end{aligned}$$

Here $\mathcal{D} \equiv d/dr$. The domain ($r = [0, 1]$) is discretised using the Chebyshev spectral collocation method [42] and solved using a public domain software, LAPACK. As gradients are large in the mixed region, a large number of grid

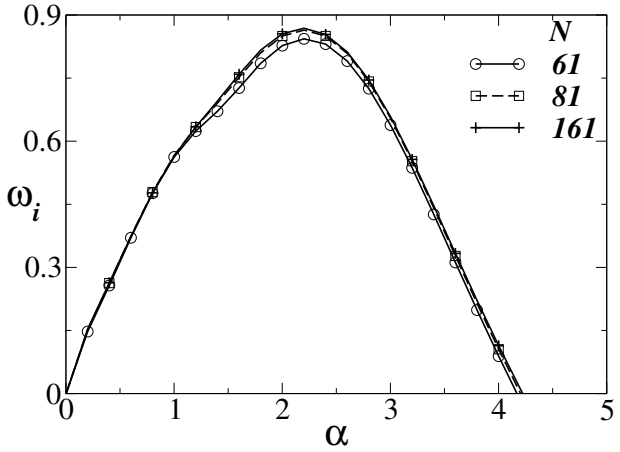

FIG. 3: The effect of increasing the order of Chebyshev polynomials, N on the dispersion curve (variation of ω_i versus α) for $Re = 1000$, $Sc = 10$, $Bn = 10$, $m = 10$, $\beta = 1$, $R_1 = 0.55$ and $q = 0.1$.

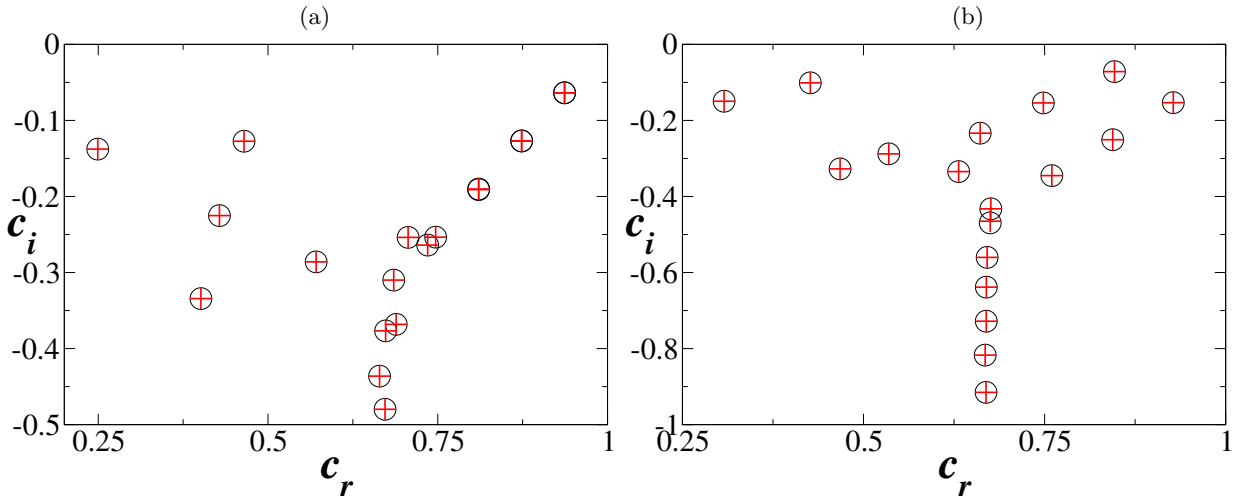

FIG. 4: Eigenspectrums for the Hagen-Poiseuille flow obtained using the present code (circles) with those given in Schmid & Henningson [40] (plus signs) for Reynolds number, Re_{SH} ($\equiv U_c \rho R/\mu_0$) = 2000: (a) $\alpha = 1$, $\beta = 0$ and (b) $\alpha = 0.5$, $\beta = 1$

points is required to compute the gradient accurately in this region. For this the following stretching function [11] is used.

$$r_j = \frac{a}{\sinh(br_0)} \left[\sinh\left\{(r_c - r_0)b\right\} + \sinh(br_0)\right], \tag{27}$$

where r_j are the locations of the grid points, a is the mid-point of the mixed layer, r_c is a Chebyshev collocation point, defined as $r_c = 0.5 \cos\left\{\left[\frac{\pi(j-1)}{(n-1)}\right] + 1\right\}$, where n is the number of collocation points. In Eq. (27),

$$r_0 = \frac{0.5}{b} \ln\left[\frac{1 + (e^b - 1)a}{1 + (e^{-b} - 1)a}\right], \tag{28}$$

and b is the degree of clustering. It is found that $b = 8$ gives an accuracy upto at least fifth decimal place in the numerically obtained growth rate (ω_i) for the range of parameters considered in this study.

D. Grid convergence test and validation of the stability solver

A grid convergence test has been conducted for a typical set of parameters used in this study. In Fig. 3, the dispersion curves (ω_i versus α) are depicted for different values of the order of Chebyshev polynomials, N for $Re = 1000$, $Sc = 10$,

$Bn = 10$, $m = 10$, $R_1 = 0.55$ and $q = 0.1$. It can be seen that the results are virtually indistinguishable for $N > 81$. Thus, the rest of the results are generated using $N = 81$. However, for most of the cases, the results are verified with those obtained using higher values of N. In order to validate the predictions of the numerical procedure, detailed comparisons with several published results for single and two-layer Newtonian fluid flows are performed. In Fig. 4, comparisons of the eigenspectrums for the Hagen-Poiseuille flow obtained using the present code (by setting $Bn = 0$ and $\mu_1 = \mu_2 = \mu_0 = 1$) with those given in Schmid & Henningson [40] for different values of the axial and azimuthal wavenumbers of the disturbance are shown. The present Reynolds number (Re) and phase speed (c) are related with those of Schmid & Henningson [40] (designated by subscript SH) as $Re = 2Re_{SH}$ and $c = 2c_{SH}$. The results agree very well. Excellent agreement is also found with the linear stability work of Sahu [43] in a core-annular flow with viscosity-stratification (not shown).

As the influences of the location of the mixed layer (R_1) and mixed layer thickness (q) have been studied by several researchers [11, 12, 43], the main objective of this study is to highlight the effects of the Bingham number (Bn), the Schmidt number (Sc) and the Newtonian viscosity ratio (m) on the stability characteristics of a core-annular flow of Newtonian and Bingham fluids.

III. RESULTS AND DISCUSSION

In Eq. (14), we observe that increasing the Newtonian viscosity ratio (m) and the Bingham number (Bn) increases the viscosity and decreases the gradient of velocity in the non-Newtonian layer (fluid '2'). Thus, first in order to study the individual effect of these parameters on the instability characteristics, one parameter is varied by keeping the other parameters fixed, i.e., effect of Bn is studied for $m = 1$, and effect of m is studied for $Bn = 0$ (Newtonian fluid). In both the cases, the rest of the parameters are $Re = 1000$, $Sc = 10$, $R_1 = 0.55$ and $q = 0.1$. The overall expected behaviours can be observed in Fig. 5(a,c) and Fig. 5(b,d), which show the basic state axial velocity (U_z) and dynamic viscosity (μ_0) profiles. It can be seen that as the values of m and Bn increase, the viscosity increases and gradient of velocity decreases in the annular region. However, there are some differences. Increasing Bn increases the viscosity of fluid '2' at $r = R_1$, but decreases it gradually for $r > R_1$ due to the increase in shear (see Fig. 5(c)). But increasing m for $Bn = 0$, increases the viscosity in region $R_1 < r < R_1 + q$ and becomes constant for $r > R_1 + q$. Note that the velocity profiles depicted in Fig. 5(a) become unphysical for $Bn > 7$, as the Bingham fluid becomes static or can have an unyielded plug at the interface for this set of parameters. As discussed in the introduction, the flow becomes stable in the presence of the unyielded region [22, 34].

The dispersion curves (ω_i versus α) associated with the corkscrew mode ($\beta = 1$) are plotted in Fig. 5(e) and (f) for different values of Bn and m, respectively. It can be seen that for $Bn = 0$ and $m = 1$ (when both the fluids are the same Newtonian fluid, i.e. the Hagen-Poiseuille flow), the growth rate, ω_i is negative for all values of α indicating that the flow is stable. It is well known that the Hagen-Poiseuille pipe flow is always linearly stable (Schmid & Henningson [40]). Increasing Bn (Fig. 5(e)) or m (Fig. 5(f)) makes the dispersion curves paraboloidal, and $\omega_i > 0$ over a finite band of wavenumbers, indicating the presence of a linear instability. It can be seen in Fig. 5(e) that increasing Bn increases the maximum growth rate, $\omega_{i,max}$. For $Bn = 7$, two peaks can be observed at $\alpha \approx 1.1$ and 1.8. On the other hand, increasing the value of m has a non-monotonic effect on the instability behaviour, i.e. $\omega_{i,max}$ increases upto $m = 20$ and then decreases for this set of parameters, as shown in Fig. 5(f). Sahu and co-workers [26, 43] also observed the non-monotonic behaviour of the viscosity ratio (m) in a core-annular pipe flow of Newtonian fluids, and in a two-layer channel flow of a non-Newtonian fluid. In Fig. 5(e), the dispersion curve (shown by blue solid line) for $Bn = 7$ is plotted by setting $R_s = R_\pi = 0$, i.e., by neglecting the viscosity perturbation terms in Eqs. (17)-(21). It can be seen that the growth rate obtained in this case is slightly higher than that obtained including the viscosity perturbations. This observation reveals that the instability in the flow is mainly due to the change in the velocity profile in the presence of the Bingham layer.

The effect of Bn and m on the stability characteristics of the axisymmetric mode ($\beta = 0$) is presented in Fig. 6(a) and (b), respectively. The rest of the parameters are the same as those used to generate Fig. 5. It can be seen in Fig. 6(a) that for $Bn \leq 5$ and $m = 1$, the flow is stable to the axisymmetric disturbance ($\beta = 0$), and for $Bn = 7$ there is positive growth of the disturbance ($\omega_i > 0$), albeit very small as compared to that associated with the corresponding corkscrew mode ($\beta = 1$). Similarly, increasing m for $Bn = 0$ increases the maximum growth rate, $\omega_{i,max}$ of the axisymmetric mode (Fig. 6(b)), but the growth rate is much smaller than the corresponding corkscrew mode (Fig. 5(f)). The stability analysis conducted by Sahu [43] also predicted that when the annular fluid is more viscous than the core fluid, the corkscrew mode ($\beta = 1$) is more unstable than the axisymmetric mode ($\beta = 0$) for the same set of the other parameters. It is also found (not shown) that the growth rate for $\beta \geq 2$ is always less than that observed for the corresponding corkscrew ($\beta = 1$) and axisymmetric ($\beta = 0$) modes.

To understand the underlying mechanism of the instability which arises due to the non-Newtonian nature of the annular fluid, an energy budget analysis similar to the one of Selvam *et al.* [20] is conducted. Here, the temporal rate

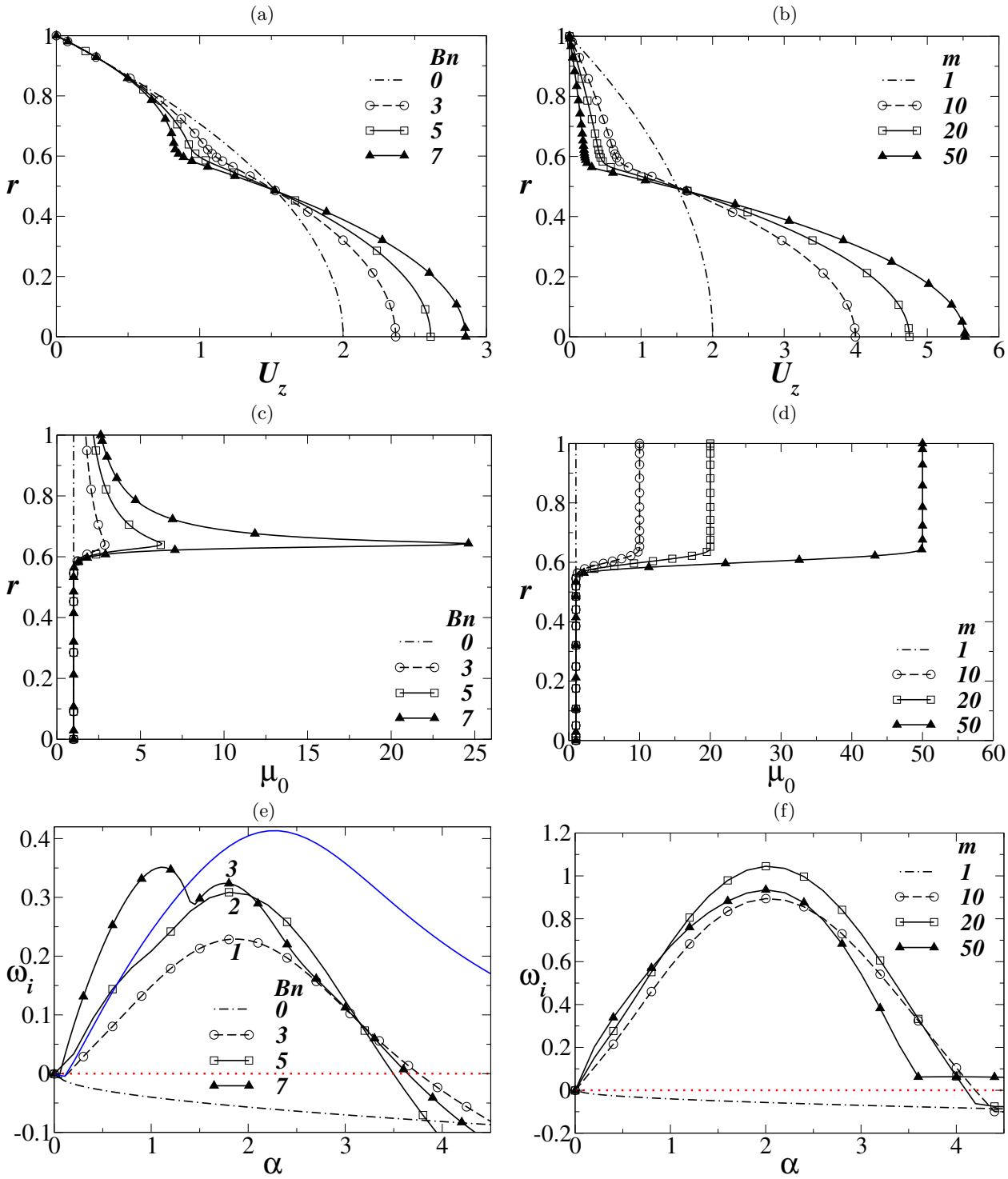

FIG. 5: (a,c,e) Effect of the Bingham number, Bn on basic state velocity (U_z) and viscosity (μ_0) profiles, and the dispersion curves (ω_i versus α) associated with the corkscrew mode ($\beta = 1$) for $m = 1$. (b,d,f) Effect of Newtonian viscosity ratio, m on basic state velocity (U_z) and viscosity (μ_0) profiles, and the dispersion curves (ω_i versus α) associated with the corkscrew mode ($\beta = 1$) for $Bn = 0$. The rest of the parameter values are $Re = 1000$, $Sc = 10$, $R_1 = 0.55$ and $q = 0.1$. The blue solid line in panel (e) shows the dispersion curve obtained for $Bn = 7$ by setting $R_s = R_\pi = 0$ in Eqs. (17)-(21).

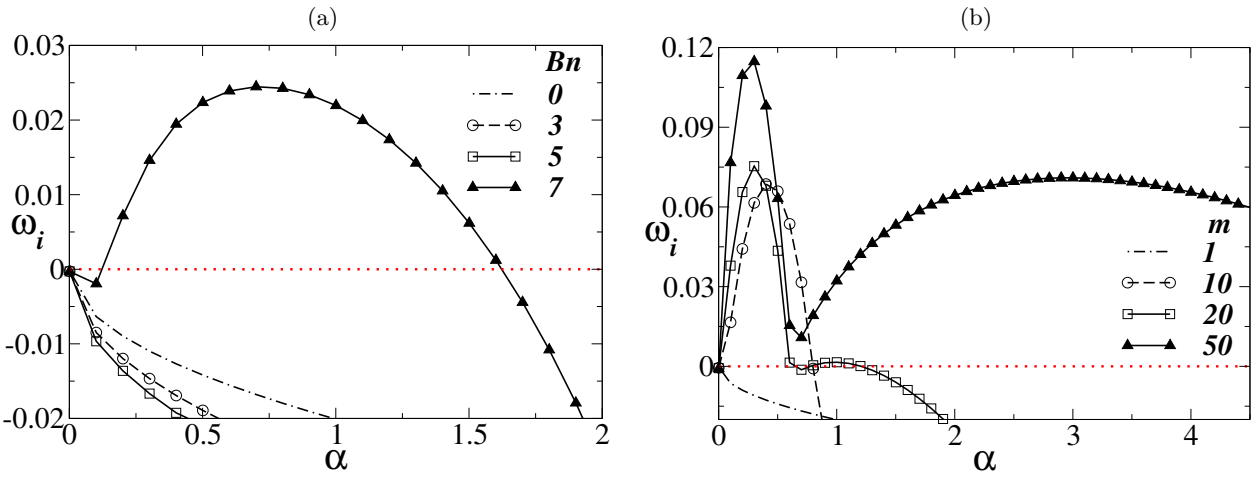

FIG. 6: Effect of (a) Bingham number, Bn for $m = 1$ and (b) the viscosity ratio, m for $Bn = 0$, on the dispersion curves (ω_i versus α) associated with the axisymmetric mode ($\beta = 0$). The rest of the parameter values are $Re = 1000$, $Sc = 10$, $R_1 = 0.55$ and $q = 0.1$.

of change of the perturbation kinetic energy, $\mathcal{E}_{int}$ is divided into different terms based on their nature of contribution to the instability.

$$\mathcal{E}_{int} = \mathcal{P}_{int} + \mathcal{D}_{int} + \mathcal{A}_{int} + \mathcal{B}_{int} + \mathcal{C}_{int}, \tag{29}$$

where

$$\mathcal{E}_{int} = \int_0^1 E r dr = \omega_i \int_0^1 \left(u_r u_r^* + u_\theta u_\theta^* + u_z u_z^*\right) r dr, \tag{30}$$

$$\mathcal{P}_{int} = \int_0^1 P_d r dr = \int_0^1 \text{Imag}\left(u_r u_z^*\right) U_z' r dr, \tag{31}$$

$$\begin{aligned}\mathcal{D}_{int} &= -\int_0^1 D r dr = -\frac{1}{Re}\int_0^1 \mu_0 \Big[u_r' u_r'^* + u_\theta' u_\theta'^* + u_z' u_z'^* \\ &+ \left(\frac{\beta^2}{r^2} + \alpha^2\right)\left(u_r u_r^* + u_\theta u_\theta^* + u_z u_z^*\right) + \frac{1}{r^2}\left\{u_r u_r^* + u_\theta u_\theta^* + 4\beta \text{Real}\left(u_\theta u_r^*\right)\right\}\Big] r dr,\end{aligned} \tag{32}$$

$$\mathcal{A}_{int} = \int_0^1 A r dr = \frac{1}{Re}\int_0^1 \frac{\mu_0'}{r}\left(\frac{d}{dr}\left(r u_r u_r^*\right) - u_\theta u_\theta^*\right) r dr, \tag{33}$$

$$\mathcal{B}_{int} = \mathcal{B}_{r int} + \mathcal{B}_{z int} = \int_0^1 B_r r dr + \int_0^1 B_z r dr = \frac{1}{Re}\int_0^1 U_z' \text{Real}\left(\mu' u_z^*\right) r dr + \frac{1}{Re}\int_0^1 U_z' \text{Real}\left(\alpha \mu u_r^*\right) r dr, \tag{34}$$

$$\mathcal{C}_{int} = \int_0^1 C r dr = \frac{dP}{dz}\int_0^1 \text{Real}\left(\mu u_z^*\right) r dr. \tag{35}$$

Here $\mathcal{P}_{int}$ represents the "Reynolds stress" term, which measures the rate of transfer of energy from the basic flow to the perturbation. $\mathcal{D}_{int}$ is the viscous dissipation of perturbation energy, $\mathcal{A}_{int}$ denotes the energy of the perturbation due to mean viscosity gradients, and $\mathcal{B}_{int}$ and $\mathcal{C}_{int}$ are the perturbation energies due to the gradient of viscosity perturbation and viscosity perturbation, respectively. $\mathcal{B}_{int}$ can be further divided into $\mathcal{B}_{r int}$ and $\mathcal{B}_{z int}$, where $\mathcal{B}_{r int}$ and $\mathcal{B}_{z int}$ are the perturbation energies associated with the gradient of viscosity perturbation in the radial and axial directions, respectively.

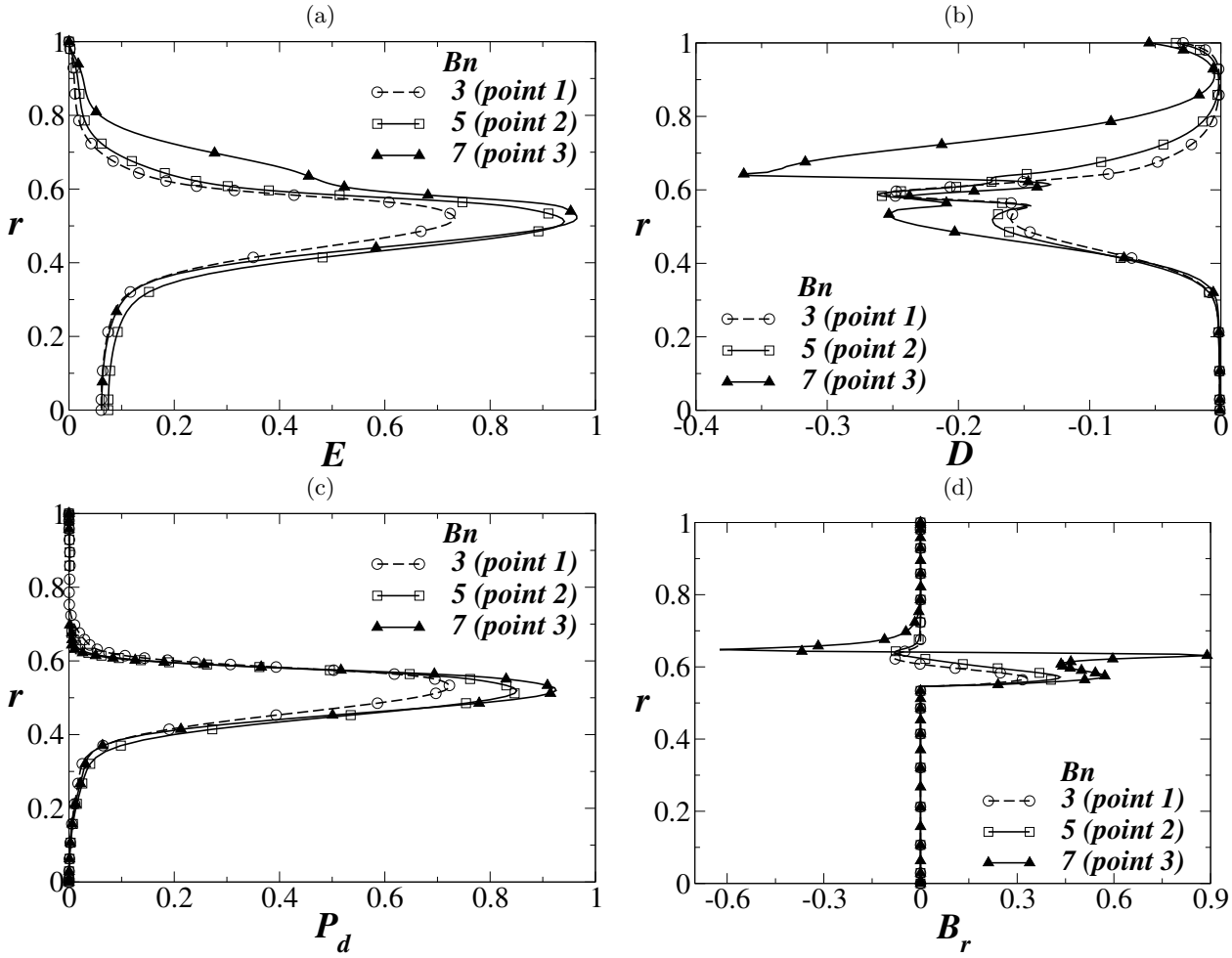

FIG. 7: Radial variations of (a) the rate of change of kinetic energy, E, (b) the dissipation rate (D), (c) the production rate, P_d and (d) B_r associated with 1 2 and 3 in Fig. 5 for different values of Bn at $\alpha = 1.9$. The rest of the parameter values are the same as those used to generate Fig. 5.

Also the terms inside the integral in Eqs. (30) - (35) are defined as $E \equiv \omega_i(u_r u_r^* + u_\theta u_\theta^* + u_z u_z^*)$, $P_d \equiv \mathrm{Imag}(u_r u_z^*)U_z'$, $D \equiv -\mu_0[u_r' u_r'^* + u_\theta' u_\theta'^* + u_z' u_z'^* + \left(\beta^2/r^2 + \alpha^2\right)(u_r u_r^* + u_\theta u_\theta^* + u_z u_z^*) + \frac{1}{r^2}\{u_r u_r^* + u_\theta u_\theta^* + 4\beta \mathrm{Real}\,(u_\theta u_r^*)\}]/Re$, $A \equiv \mu_0'(d/dr\,(r u_r u_r^*) - u_\theta u_\theta^*)/Re/r$, $B_r \equiv U_z' \mathrm{Real}(\mu' u_z^*)/\mathrm{Re}$, $B_z \equiv U_z' \mathrm{Real}(\alpha \mu u_r^*)/Re$ and $C \equiv (dP/dz)\mathrm{Real}\,(\mu u_z^*)$.

The radial variations of E and the dominant energy terms, i.e., D, P_d and B_r associated with point 1, 2 and 3 in Fig. 5(e) are plotted for different values of Bn in Fig. 7(a), (b), (c) and (d), respectively. It can be seen that the energy due to the gradient of viscosity perturbation in the radial direction (B_r) is zero everywhere, except near the mixed layer. It can be seen that below $r \approx 0.6$, B_r is positive, but above $r \approx 0.6$, B_r is negative. The production due to the transfer of energy from the basic flow to the perturbation (P_d) is positive, whereas the viscous dissipation (D) is negative everywhere. However, the combined positive contribution from P_d and B_r is more than the negative viscous dissipation for this set of parameter values, which increases with increasing in Bn, thereby destabilising the flow.

In order to understand the stability behaviour of the flow in the inviscid limit ($Re \to \infty$), an inviscid analysis is also conducted. Based on this, a pipe flow is inviscidly unstable if the inviscid stability function, $I \equiv U_z'' - U_z'(\alpha^2 r^2 - \beta^2)/r/(\alpha^2 r^2 + \beta^2)$ corresponds to the most dangerous mode changes its sign inside the domain [44]. This is analogous to the Rayleigh's inviscid stability criteria of planar flows [45]. The radial variations of the inviscid stability function, I associated with 1 2 and 3 in Fig. 5(e) for different values of Bn at $\alpha = 1.9$ are plotted in Fig. 8. It can be seen that for all values of Bn considered, I changes sign in the mixed region ($0.55 \leq r \leq 0.65$) for this set of parameters. This indicates that the mechanism of the instability observed in the present study is inviscid in nature. Thus, we will see later in this article that unlike in case core-annular flow of Newtonian fluids [43], the neutral stability curves do not close at a high Reynolds number.

After identifying the mechanism of the instability, in the rest of the study, the effects of Bn, Sc and m are

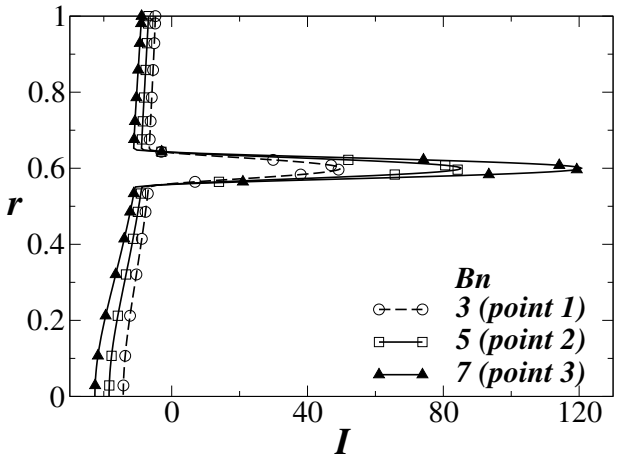

FIG. 8: Radial variations of the inviscid instability function, I associated with points 1 2 and 3 in Fig. 5(e) for different values of Bn at $\alpha = 1.9$. The rest of the parameter values are the same as those used to generate Fig. 5.

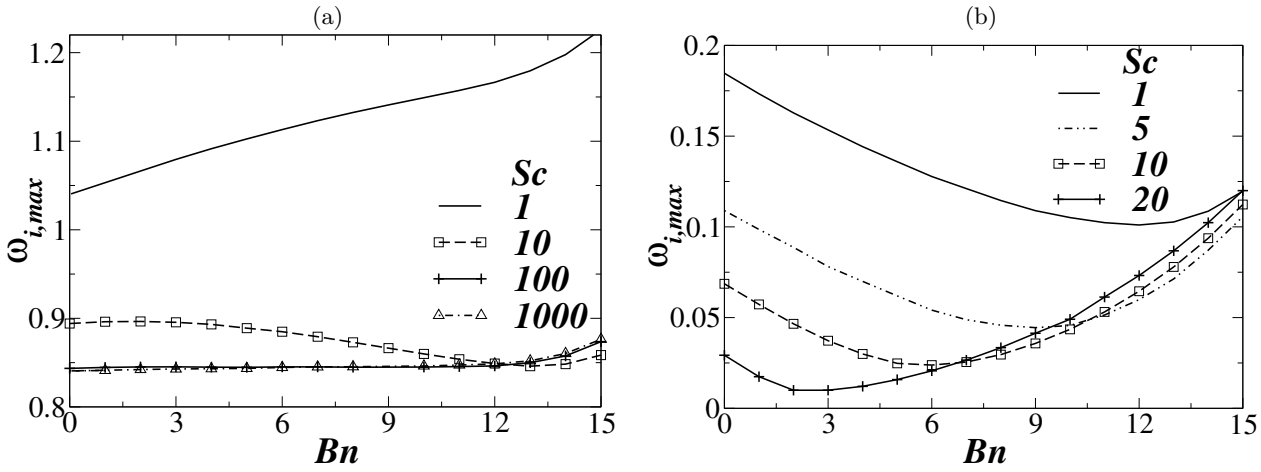

FIG. 9: Variation of $\omega_{i,max}$ versus Bn for different values of Sc. (a) Corkscrew mode ($\beta = 1$), and (b) axisymmetric mode ($\beta = 0$). The rest of the parameter values are $Re = 1000$, $R_1 = 0.55$, $q = 0.1$ and $m = 10$.

investigated for both corkscrew ($\beta = 1$) and axisymmetric ($\beta = 0$) modes. The rest of the parameter values are fixed at $Re = 1000$, $R_1 = 0.55$, and $q = 0.1$. The variations of the maximum temporal growth rate, $\omega_{i,max}$ versus Bn for $m = 10$ are plotted for different values of Schmidt number in Fig. 9(a) and (b), which correspond to the corkscrew and axisymmetric modes, respectively. It can be seen that for $Bn = 0$ (Newtonian case), increasing Sc decreases the value of $\omega_{i,max}$. This behaviour is observed for both the corkscrew and axisymmetric modes. In Fig. 9(a) (corkscrew mode) for $Sc = 1$, it is observed that increasing Bn increases $\omega_{i,max}$ significantly, whereas for $Sc = 10$, the maximum growth rate decreases upto $Bn \approx 12.4$ and then increases slightly. But for $Sc = 100$, the maximum growth rate remains constant upto $Bn \approx 12.4$ and increases for $Bn > 12.4$. Frigaard *et al.* [22] also observed that Bn has a stabilising influence in single Bingham fluid flow in a two-dimensional channel. The stability behaviour observed for the axisymmetric mode ($\beta = 0$) for $m = 10$ (see Fig. 9(b)) is opposite to that of the corkscrew mode ($\beta = 1$). In this case, increasing Bn decreases and then increases the value of $\omega_{i,max}$ for all Sc considered. The value of this crossover Bn increases with decreasing Sc. However, the values of $\omega_{i,max}$ for the axisymmetric mode are much smaller than those correspond to the corkscrew mode, which indicates that the corkscrew mode ($\beta = 1$) is the most dominant mode for the instability in the present case.

The variations of $\omega_{i,max}$ versus Bn are plotted for $m = 2$ in Fig. 10(a) and (b) for the corkscrew ($\beta = 1$) and axisymmetric ($\beta = 0$) modes, respectively. In Fig. 10(a) (corkscrew mode), it can be seen that $\omega_{i,max}$ increases with increasing Bn. It can be seen that for $Sc = 1$, increasing Bn increases $\omega_{i,max}$. For other values of Sc, increase in Bn has a non-monotonic effect; increasing Bn increases $\omega_{i,max}$ initially, followed by a slight decrease in its value and then subsequently increases at a faster rate. This behaviour is more evident for $Sc = 100$ and 1000. Further, the

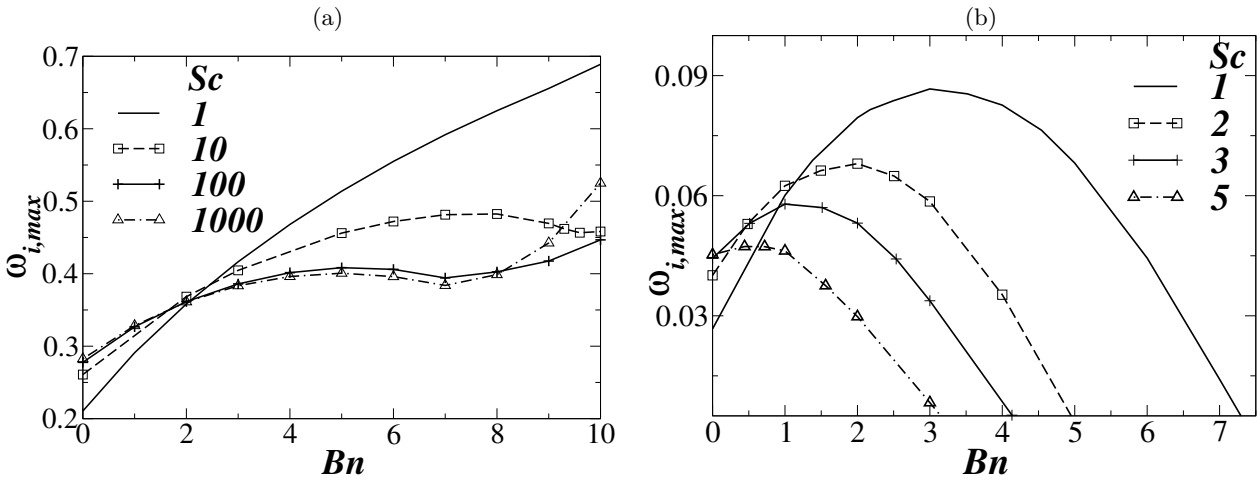

FIG. 10: Variation of $\omega_{i,max}$ versus Bn for different values of Sc. (a) Corkscrew mode ($\beta = 1$) and (b) axisymmetric mode ($\beta = 0$). The rest of the parameter values are $Re = 1000$, $R_1 = 0.55$, $q = 0.1$ and $m = 2$.

instability behaviour for the corkscrew mode ($\beta = 1$) can be classified into two regimes, for $Bn < 2$ and $Bn > 2$ (approximately). For $Bn < 2$, increasing Sc increases the value of $\omega_{i,max}$ (destabilising), whereas for $Bn > 2$, the instability behaviour with increasing Sc is opposite (stabilising). The stability characteristics for the axisymmetric mode ($\beta = 0$) presented in Fig. 10(b) for $m = 2$ reveals that increasing Sc decreases the value of $\omega_{i,max}$; thus has a stabilising influence.

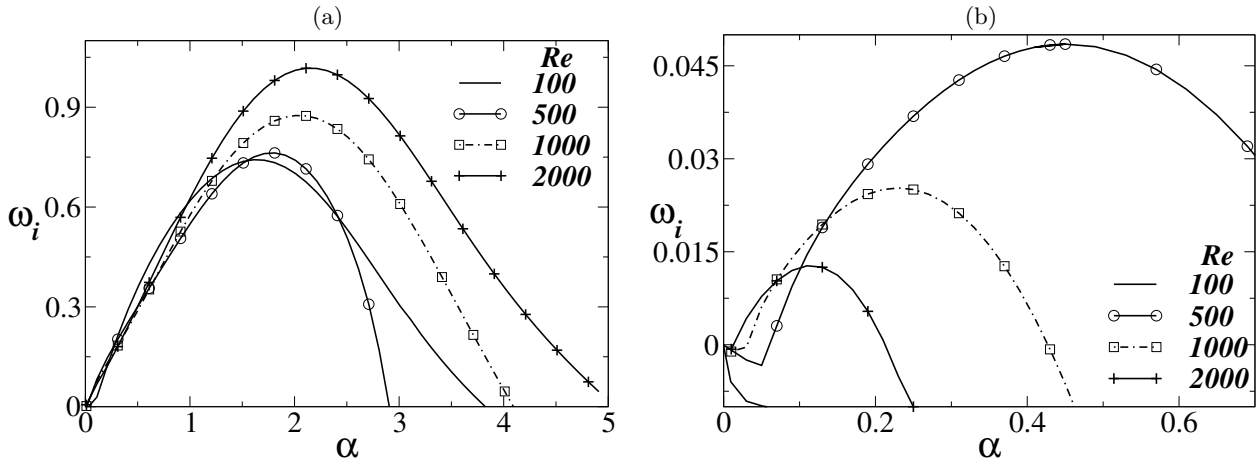

FIG. 11: Effect of Reynolds number, Rn on the growth rate for (a) $\beta = 1$ and $\beta = 0$. The rest of the parameter values are $m = 10$, $Bn = 5$, $Sc = 10$, $R_1 = 0.55$ and $q = 0.1$.

The effects of Reynolds number on the dispersion curves for $\beta = 1$ and $\beta = 0$ are shown in Fig. 11(a) and (b), respectively. The rest of the parameter values are $m = 10$, $Bn = 5$, $Sc = 10$, $R_1 = 0.55$ and $q = 0.1$. It can be observed that for all Re values considered the corkscrew mode ($\beta = 1$) is the most unstable mode, and as expected, increasing Re increases the maximum growth rate of the most unstable mode associated with $\beta = 1$. However, we can see some non-monotonic trend in growth rate for the axisymmetric mode ($\beta = 0$), but the maximum growth rate for $\beta = 0$ for each Re value is two order of magnitude less than the corresponding growth rate observed for $\beta = 1$.

Inspection of Figs. 9, 10 and 11 also reveals that, for the range of parameters considered, the values of $\omega_{i,max}$ are much smaller for the axisymmetric mode than those correspond to the corkscrew mode, which indicates that the corkscrew mode ($\beta = 1$) is the most dominant mode. Thus, in Fig. 12, the neutral stability curves (contours of $\omega_i = 0$ in Re and α space) separating the stable and unstable regions are shown for different values of Bn for $\beta = 1$. The rest of the parameter values are $Sc = 10$, $R_1 = 0.55$, $q = 0.1$ and $m = 2$. Here also it can be seen that Bn has a destabilising influence, i.e. increasing Bn decreases the value of Re below which flow is stable (known as critical Reynolds number).

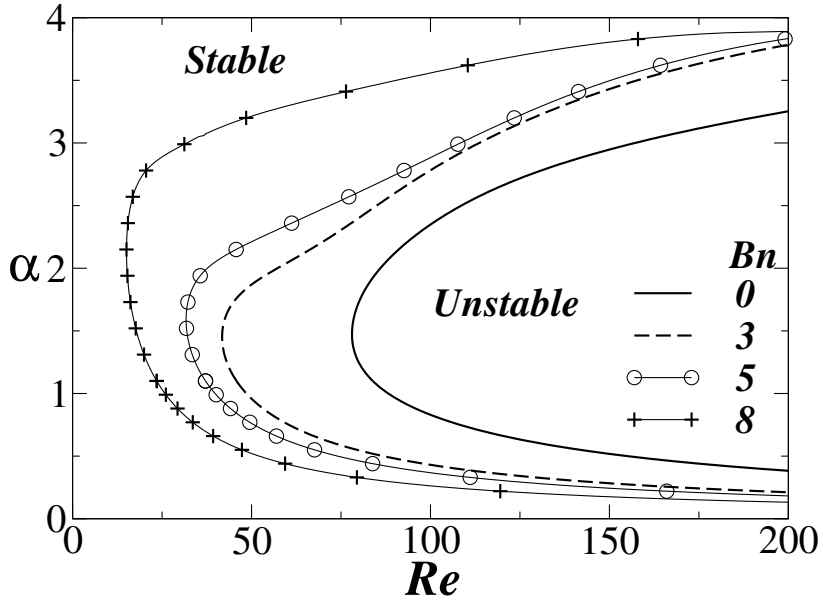

FIG. 12: Neutral stability curves at different values of Bn associated with the corkscrew mode ($\beta = 1$). The rest of the parameter values are $Sc = 10$, $R_1 = 0.55$, $q = 0.1$ and $m = 2$.

IV. CONCLUDING REMARKS

In this work, the instability characteristics of a core-annular pipe flow of a Newtonian fluid and a Bingham fluid is investigated via a normal-mode linear stability analysis of three-dimensional disturbances. The fluids are assumed to be miscible, which is characterised by the Schmidt number. A parallel flow approximation (valid for large Péclet number, $Pe = ReSc$) is employed such that the fluids are assumed to be separated by a mixed layer of uniform thickness. As the effects of the location and thickness of the mixed region have investigated throughly in the past, the main emphasis of this study is to investigate the effect of the non-Newtonian nature (yield stress/Bingham number) of the annular fluid. A energy budget and inviscid stability analysis are conducted to understand the underlying mechanism of the instability due to the non-Newtonian nature of the annular fluid. The following conclusions can be drawn from this study. For the parameters considered in the present study (for which the entire flow is yielded), (i) the corkscrew mode is more unstable than the corresponding axisymmetric mode. (ii) The Bingham number destabilises the dominant corkscrew mode via changing the basic state profile. In the presence of unyielded region, however, the flow is stable as shown by Frigaard and co-workers [22, 34]. A parametric study is conducted to analyse the influence of the Schmidt number, Reynolds number and the Bingham number for $m = 2$ and $m = 10$. As expected, increasing Re destabilises the flow. It is observed that $\omega_{i,max}$ of the corkscrew mode increases monotonically with increasing Re. It is found that for both the viscosity ratios considered, in case of high diffusivity ($Sc = 1$), increasing Bn destabilises the flow, i.e. maximum growth rate ($\omega_{i,max}$) associated with the corkscrew mode increases significantly. For intermediate diffusivity ($Sc = 10$), it is found that increasing Bn decreases $\omega_{i,max}$ till a certain value of Bn and then increases slightly for $m = 10$. The opposite happens for the low viscosity ratio ($m = 2$). In this case increasing Bn increases $\omega_{i,max}$ upto $Bn \approx 8$ and then decreases the value of $\omega_{i,max}$ slightly. For low diffusive case (high Sc), increasing Bn has a destabilising influence. The critical Reynolds number also decreases with increasing Bn for the corkscrew mode. It is found that an inviscid mechanism is operational in this case.

Acknowledgement: The author thanks Department of Science & Technology, India for providing financial support through the grant number, MTR/2017/000029.

Appendix: Justification for the basic flow

Consider a situation when a splitter plate is located at $z < 0$, at a constant r and the parallel streams of two miscible fluids flow on both sides of this plate. The streams come in to contact with each other at $z = z_0$. The two fluids begin to mix with each other for $z > 0$, thus producing a stratified layer. The thickness 'q' of this layer grows as the fluids move downstream and therefore q is a function of z.

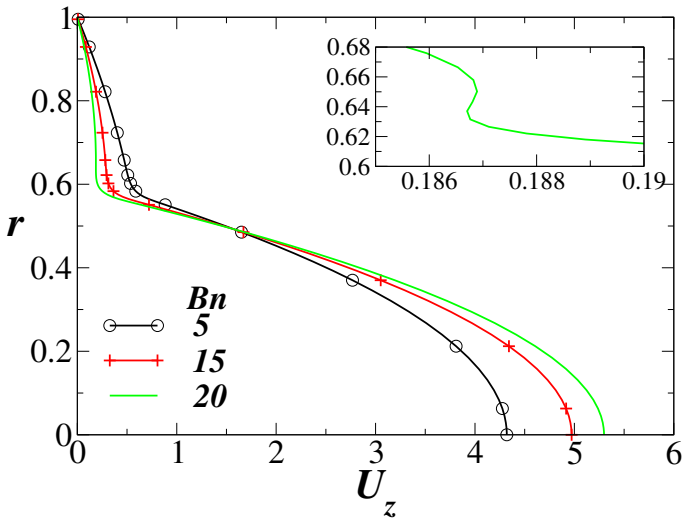

FIG. 13: Basic state profiles for different values of Bn. The parameters are the same as those used to generate Fig. 2. The inset represents the zoomed view of the profile for $Bn = 20$ in the interfacial region.

We know at any location, s_0 satisfies Eq. (9), which is given by

$$\frac{\partial s_0}{\partial t} + U_r \frac{\partial s_0}{\partial r} + U_z \frac{\partial s_0}{\partial z} = \frac{1}{ReSc}\left[\frac{\partial^2 s_0}{\partial r^2} + \frac{1}{r}\frac{\partial s_0}{\partial r} + \frac{\partial^2 s_0}{\partial z^2}\right]. \tag{36}$$

The splitter imposes no-slip on the fluids on either side of the streams as soon as they leave the splitter plate and the velocity profile goes through a spatially developing region (entry region). In this region, the velocity profile will be a strong function of axial coordinate, z (the same order as the radial variation). Thus, the locally parallel assumption used in the present study is valid only after this developing region and for slow diffusion (i.e for high $Pe \equiv ReSc$). Slow diffusion means that the time scale of diffusion is much smaller than the flow time scale. Based on this approximation and boundary layer assumption, we can say that $u_r \ll u_z$ and $\partial/\partial z \ll \partial/\partial r$. Comparing the order of magnitude of the terms in Eq. (36), we get, if $U_z = \mathcal{O}(1)$ then $U_r = \mathcal{O}(1/Pe)$, $\partial s_0/\partial r = \mathcal{O}(1)$ and $\partial s_0/\partial z = \mathcal{O}(1/Pe)$. Thus under the parallel flow approximation, and after the fluids cross the developing region, Eq. (36) reduces to

$$\frac{\partial s_0}{\partial t} = \frac{1}{ReSc}\left[\frac{1}{r}\frac{\partial}{\partial r}\left(r\frac{\partial s_0}{\partial r}\right)\right]. \tag{37}$$

The solution of Eq. (37) is an error function. It is found that a fifth order polynomial as used in the present study is also a good representation of the error function. After Tan & Homsy [46], several authors have used the quasi-steady approximation to represent a basic concentration profile in the form of a hyperbolic tangent (Ern *et al.* [39]) or an error function (e.g. Meiburg and co-workers [20, 47]). Some have also used a fifth-order polynomial (see e.g. Malik and Hooper [48], Govindarajan *et al.*, [49]), which is smooth enough to approximate the concentration profile. The basic state considered in this work can also be viewed in a frame moving with the interface speed such that the flow is dominated by diffusive and s_0 is governed by Eq. (37).

Previously we [38] have compared the viscosity profiles obtained using s_0 represented by an error function and a hyperbolic tangent, and the stability behaviours associated them, and found that the results are indistinguishable. From the stability analysis point of view, this can be interpreted as the radial gradients of the flow variables and the thickness q of the mixed region have much larger length scale than the wavelength of the unstable disturbances. The result obtained from a linear stability analysis for a three-layer channel flow performed using locally parallel flow assumption was found to be in good agreement with that of the direct numerical simulation [43, 50]. In these studies, the basic state and the linear stability behaviour of a miscible fluids flow obtained using locally parallel flow assumption have been compared with direct numerical simulation. The agreement was very good, see for instance Fig. 14 of Ref. [43].

Now coming to the unphysical nature of the basic state profile for high Bn, as discussed in Section II, for a given set of dimensionless parameters, as the value of Bn exceeds a critical value (Bn_{cr}), the velocity profile becomes unphysical as can be seen in Fig. 13. It can be seen that when $Bn < Bn_{cr}$ for a typical set of parameters, the velocity, U_z decreases continuously as we move from the centerline towards the wall (see the profiles for $Bn = 5$

and 15 in Fig. 13). But for $Bn > Bn_{cr}$, with the increase in r, the velocity, U_z decreases till the interfacial region, then increases slightly (see the zoomed view for $Bn = 20$) and finally decreases again as we move towards the wall. Physically, U_z can not exhibit a non-monotonic behaviour like the one we see for $Bn = 20$ for this set of parameters. Thus, the rheological model used is valid only for $Bn < Bn_{cr}$.

Acknowledgement: The author sincerely thanks the anonymous reviewers for their many insightful comments and suggestions.

---

[1] R. Govindarajan and K. C. Sahu, "Instabilities in viscosity-stratified flows," Ann. Rev. Fluid Mech. **46**, 331 (2014).
[2] D. D. Joseph, R. Bai, K. P. Chen, and Y. Y. Renardy, "Core-annular flows," Ann. Rev. Fluid Mech. **29**, 65 (1997).
[3] Q. Cao, L. Ventresca, K. R. Sreenivas, and A. K. Prasad, "Instability due to viscosity stratification downstream of a centreline injector," Can. J. Chem. Eng. **81**, 913 (2003).
[4] R. B. Bird, G. Dai, and B. J. Yarusso, "The rheology and flow of viscoplastic materials," Rev. Chem. Eng. **1**, 1 (1983).
[5] P. Coussot, "Yield stress fluid flows: A review of experimental data," J. Non-Newtonian Fluid Mech. **211**, 31 (2014).
[6] C. S. Yih, "Instability due to viscous stratification," J. Fluid Mech. **27**, 337 (1967).
[7] C. E. Hickox, "Instability due to viscosity and density stratification in axisymmetric pipe flow," Phys. Fluids **14**, 251 (1971).
[8] D. D. Joseph, M. Renardy, and Y. Y. Renardy, "Instability of the flow of two immiscible liquids with different viscosities in a pipe," J. Fluid Mech. **141**, 309 (1984).
[9] C. Kouris and J. Tsamopoulos, "Dynamics of axisymmetric core-annular flow in a straight tube. I. The more viscous fluid in the core, bamboo waves," Phys. Fluids **13**, 841 (2001).
[10] C. Kouris and J. Tsamopoulos, "Dynamics of axisymmetric core-annular flow in a straight tube. II. The less viscous fluid in the core, saw tooth waves," Phys. Fluids **14**, 1011 (2002).
[11] R. Govindarajan, "Effect of miscibility on the linear instability of two-fluid channel flow," Int. J. Multiphase Flow **30**, 1177 (2004).
[12] B. T. Ranganathan and R. Govindarajan, "Stabilisation and destabilisation of channel flow by location of viscosity-stratified fluid layer," Phys. Fluids. **13(1)**, 1 (2001).
[13] K. C. Sahu, H. Ding, P. Valluri, and O. K. Matar, "Linear stability analysis and numerical simulation of miscible channel flows," Phys. Fluids **21**, 042104 (2009).
[14] K. C. Sahu and R. Govindarajan, "Linear stability of double-diffusive two-fluid channel flow," J. Fluid Mech. **687**, 529 (2011).
[15] E. Lajeunesse *et al.*, "Miscible displacement in a Hele-Shaw cell at high rates," J. Fluid Mech. **398**, 299 (1999).
[16] E. Lajeunesse, J. Martin, N. Rakotomalala, and D. Salin, "3D instability of miscible displacements in a Hele-Shaw cell," Phys. Rev. Lett. **79**, 5254 (1997).
[17] J. Scoffoni, E. Lajeunesse, and G. M. Homsy, "Interface instabilities during displacement of two miscible fluids in a vertical pipe," Phys. Fluids **13**, 553 (2001).
[18] B. Selvam, L. Talon, L. Lesshafft, and E. Meiburg, "Convective/absolute instability in miscible core-annular flow. Part 2. Numerical simulations and nonlinear global modes," J. Fluid Mech. **618**, 323 (2009).
[19] M. d'Olce *et al.*, "Pearl and mushroom instability patterns in two miscible fluids core annular flows," Phys. Fluids **20**, 024104 (2008).
[20] B. Selvam, S. Merk, R. Govindarajan, and E. Meiburg, "Stability of miscible core-annular flows with viscosity stratification," J. Fluid Mech. **592**, 23 (2007).
[21] I. A. Frigaard, "Super-stable parallel flows of multiple visco-plastic fluids," J. Non-Newt. Fluid Mech. **100**, 49 (2001).
[22] I. A. Frigaard, S. D. Howison, and I. J. Sobey, "On the stability of Poiseuille flow of a Bingham fluid," J. Fluid Mech. **263**, 133 (1994).
[23] A. Pinarbasi and A. Liakopoulos, "Stability of two-layer Poiseulle flow of Carreau-Yasuda and Bingham-like fluids," J. Non-Newt. Fluid Mech. **57**, 227 (1995).
[24] I. Frigaard and C. Nouar, "On three-dimensional linear stability of Poiseuille flow of Bingham fluids," Phys. Fluids **15 (10)**, 2843 (2003).
[25] K. C. Sahu and O. K. Matar, "Three-dimensional linear instability in pressure-driven two-layer channel flow of a Newtonian and a Herschel-Bulkley fluid," Phys. Fluids **22**, 112103 (2010).
[26] K. C. Sahu, P. Valluri, P. D. M. Spelt, and O. K. Matar, "Linear instability of pressure-driven channel flow of a Newtonian and Herschel-Bulkley fluid," Phys. Fluids **19**, 122101 (2007).
[27] M. Escudier and F. Presti, "Pipe flow of a thixotropic liquid," J. Non-Newtonian Fluid Mech. **62**, 291 (1996).
[28] M. Escudier *et al.*, "Observations of asymmetrical flow behaviour in transitional pipe flow of yield-stress and other shear-thinning liquids," J. Non-Newtonian Fluid Mech. **127**, 143 (2005).
[29] J. Peixinho, C. Nouar, C. Desaubry, and B. Théron, "Laminar transitional and turbulent flow of yield stress fluid in a pipe," J. Non-Newtonian Fluid Mech. **128**, 172 (2005).
[30] A. Esmael and C. Nouar, "Transitional flow of a yield-stress fluid in a pipe: Evidence of a robust coherent structure," Phys. Rev. E. **77**, 057302 (2008).

[31] B. Güzel, T. Burghelea, I. A. Frigaard, and D. Martinez, "Observation of laminar–turbulent transition of a yield stress fluid in Hagen–Poiseuille flow," J. Fluid Mech. **627**, 97 (2009).
[32] S. Hormozi and I. Frigaard, "Nonlinear stability of a visco-plastically lubricated viscoelastic fluid flow," J. Non-Newtonian Fluid Mech. **169**, 61 (2012).
[33] M. Moyers-Gonzalez, I. Frigaard, and C. Nouar, "Nonlinear stability of a visco-plastically lubricated viscous shear flow," J. Fluid Mech. **506**, 117 (2004).
[34] S. Hormozi, K. Wielage-Burchard, and I. Frigaard, "Entry, start up and stability effects in visco-plastically lubricated pipe flows," J. Fluid Mech. **673**, 432 (2011).
[35] S. Ghosh, R. Usha, and K. C. Sahu, "Double-diffusive two-fluid flow in a slippery channel: A linear stability analysis," Phys. Fluids. **26**, 015412 (2014).
[36] E. Bingham, "An Investigation of the Laws of Plastic Flow," US Bureau of Standards Bulletin. **13**, 309 (1916).
[37] W. H. Herschel and R. Bulkley, "Konsistenzmessungen von gummi-benzollösungen," Colloid & Polymer Science **39**, 291 (1926).
[38] K. C. Sahu and R. Govindarajan, "Instability of a free-shear layer in the vicinity of a viscosity-stratified layer," J. Fluid Mech. **752**, 626 (2014).
[39] P. Ern, F. Charru, and P. Luchini, "Stability analysis of a shear flow with strongly stratified viscosity," J. Fluid Mech. **496**, 295 (2003).
[40] P. J. Schmid and D. S. Henningson, *Stability and transition in shear flows* (Springer-Verlag New York, Inc, New York, 2001).
[41] M. R. Khorrami, M. R. Malik, and R. L. Ash, "Application of spectral collocation techniques to the stability of swirling flows," J. Comput. Phys **81**, 206 (1989).
[42] C. Canuto, M. Y. Hussaini, A. Quarteroni, and T. Zang, *Spectral Methods in Fluid Dynamics*, 1st ed. (Springer-Verlag, Amsterdam, 1987), pp. 65–70.
[43] K. C. Sahu, "Double-diffusive instability in core–annular pipe flow," J. Fluid Mech. **789**, 830 (2016).
[44] K. C. Sahu and R. Govindarajan, "Stability of flow through a slowly diverging pipe," J. Fluid Mech. **531**, 325 (2005).
[45] L. Rayleigh, "On the stability of certain fluid motions," Proc. Math. Soc. Lond. **11**, 57 (1880).
[46] C. T. Tan and G. M. Homsy, "Stability of miscible displacements: rectangular flow," Phys. Fluid **29**, 73549 (1986).
[47] L. Talon and E. Meiburg, "Plane Poiseuille flow of miscible layers with different viscosities: instabilities in the Stokes flow regime," J. Fluid Mech. **686**, 484 (2011).
[48] S. V. Malik and A. P. Hooper, "Linear stability and energy growth of viscosity stratified flows," Phys. Fluids **17**, 024101 (2005).
[49] R. Govindarajan, S. V. L'vov, and I. Procaccia, "Retardation of the onset of turbulence by minor viscosity contrasts," Phys. Rev. Lett. **87**, 174501 (2001).
[50] K. C. Sahu and R. Govindarajan, "Linear stability analysis and direct numerical simulation of two layer channel flow," J. Fluid Mech. **798**, 889-909 (2016).
[51] D. D. Joseph and Y. Y. Renardy, "Fundamentals of two-fluid dynamics: Part i: Mathematical theory and applications," Springer Science & Business Media, **3** (2013).
[52] D. D. Joseph and Y. Y. Renardy, "Fundamentals of two-fluid dynamics. Pt. II: Lubricated transport, drops and miscible liquids," Springer Science & Business Media, **4** (1993).